communications biology

Article

https://doi.org/10.1038/s42003-024-06602-x

Fibroblast growth receptor 1 is regulated by G-quadruplex in metastatic breast cancer

Hang Lin[1,8], Muhammad Hassan Safdar[1,8], Sarah Washburn[1], Saeed S. Akhand[1], Jonathan Dickerhoff[1], Mitchell Ayers[1], Marvis Monteiro[1,2], Luis Solorio[3,4], Danzhou Yang[1,3,5] ✉ & Michael K. Wendt[1,3,6,7] ✉

Limiting cellular plasticity is of key importance for the therapeutic targeting of metastatic breast cancer (MBC). Fibroblast growth receptor (FGFR) is a critical molecule in cellular plasticity and potent inhibitors of FGFR enzymatic activity have been developed, but kinase independent functions for this receptor also contribute to MBC progression. Herein, we evaluated several FGFR inhibitors and find that while FGFR-targeted kinase inhibitors are effective at blocking ligand-induced cell growth, dormant cells persist eventually giving rise to MBC progression. To more broadly target FGFR and cellular plasticity, we examined the *FGFR1* proximal promoter, and found several sequences with potential to form G-quadruplex secondary structures. Circular dichroism was used to verify formation of G-quadruplex in the *FGFR1* proximal promoter. Importantly, use of the clinical G-quadruplex-stabilizing compound, CX-5461, stabilized the *FGFR1* G-quadruplex structures, blocked the transcriptional activity of the *FGFR1* proximal promoter, decreased FGFR1 expression, and resulted in potent inhibition of pulmonary tumor formation. Overall, our findings suggest G-quadruplex-targeted compounds could be a potential therapeutic strategy to limit the cellular plasticity of FGFR1 overexpressing MBC.

Metastatic breast cancer (MBC) is the most advanced stage of the disease leading to the majority of breast cancer-related deaths[1]. However, the mechanisms that govern MBC progression remain unclear, hindering development of effective treatments. Receptor tyrosine kinases (RTKs) can become constitutively activated through mutation, fusion, and gene amplification events and in this setting, active-site binding kinase inhibitors have become a mainstay of cancer therapy[2]. Wild-type RTKs still play key roles in tumor progression and metastasis through integration of signals from the tumor microenvironment[3]. Thirteen percent of breast cancer patients have amplification of the fibroblast growth factor receptor 1 (*FGFR1*) locus on chromosome 8p12, and this event correlates with decreased patient survival[4]. Furthermore, the percentage of *FGFR1* amplification increases to 26% in breast cancer metastases[5]. Expression of FGFR1 is also upregulated during epithelial-mesenchymal transition (EMT), which is a key driver of cancer metastasis[6]. Additionally, FGFR1 signaling can stabilize Twist, an EMT-related transcription factor, and propagate drug-persistent, mesenchymal subpopulations[7]. Previous findings by our lab and others demonstrate that genetic depletion of FGFR1 hinders pulmonary metastasis[8,9]. However, unlike urothelial and bile duct carcinomas where FGFRs become mutationally activated, clinical studies demonstrate minimal response to FGFR kinase inhibitors in *FGFR1*-amplified BC patients[10–13].

In addition to its kinase activity, nuclear trafficking and other non-enzymatic functions of FGFR have been proposed in breast and pancreatic cancer[14,15]. For instance, *FGFR1* has been found to localize in the nucleus of cells invading through 3D matrixes and in patient samples of invasive BC[16]. Concordant with these observations, our previous studies demonstrate that during EMT, FGFR1 disassociates from E-cadherin and can translocate to the nucleus[8]. Given these findings, therapeutic approaches of targeting total FGFR1 expression as opposed to only blockade of kinase function are being pursued[17].

G-quadruplex are noncanonical, four-stranded secondary structures of DNA or RNA. They consist of stacked planar G-tetrads, which are four

[1]Borch Department of Medicinal Chemistry and Molecular Pharmacology, Purdue University, West Lafayette, IN, USA. [2]Department of Internal Medicine, University of Iowa, Iowa City, IA, USA. [3]Purdue Institute for Cancer Research, Purdue University, West Lafayette, IN, USA. [4]Department of Biomedical Engineering, Purdue University, West Lafayette, IN, USA. [5]Department of Chemistry, Purdue University, West Lafayette, IN, USA. [6]Holden Comprehensive Cancer Center, University of Iowa, Iowa City, IA, USA. [7]Present address: Department of Internal Medicine, University of Iowa, Iowa City, IA, USA. [8]These authors contributed equally: Hang Lin, Muhammad Hassan Safdar. ✉e-mail: yangdz@purdue.edu; mkwendt@uiowa.edu

guanines connected via Hoogsteen hydrogen bonds[18]. G-quadruplex commonly form in the promoter regions of oncogenes. For instance, G-quadruplex are known to characterize the proximal promoter regions of *c-Myc* and *PDGFR*[19–22]. Resolution of the G-quadruplex is required for efficient transcription. Given their potential to restrict oncogenic gene expression and influence DNA damage repair, small molecules capable of binding to and stabilizing G-quadruplex have attracted significant attention as a promising therapeutic approach in cancer[23–26]. Some of these molecules have progressed to clinical evaluation, representing a new category of epigenetic therapies[27,28].

Herein, we present an in-depth evaluation of several FGFR kinase inhibitors. These studies clearly depict the efficacy of kinase inhibition to block ligand-induced cell growth, but also demonstrate failure to eliminate residual *FGFR1*-amplified breast cancer cells. Evaluation of the proximal promoter of *FGFR1* revealed G-quadruplex forming sequences. Application of the G-quadruplex stabilizing small molecule, CX-5461, robustly inhibited FGFR1 expression and limited pulmonary tumor progression. Overall, this work supports the hypothesis that G-quadruplex stabilization could be an effective strategy for the treatment of MBC in part through diminished expression of FGFR1.

Results

Inhibition of FGFR kinase activity suppresses tumor growth but fails to eliminate residual breast cancer cells

To investigate the efficacy of targeting FGFR kinase activity in MBC, we first utilized the murine 4T07 tumor model. When delivered to the lungs of fully immune-competent Balb/C mice via tail vein injection, these cells quickly form pulmonary tumors[29]. In our previous studies, treatment of mice bearing 4T07 pulmonary tumors with 100 mg/ml of the FDA-approved FGFR inhibitor, erdafitinib reduced tumor growth, although minimal residual disease was still detectable, and this dose caused significant weight loss in the animals, limiting treatment duration[30]. Here, we used 50 mg/ml of erdafitinib, a concentration that allowed for continuous treatment, reduced toxicity, still significantly slowed tumor growth, and extended the survival time of these animals (Fig. 1A–C). However, consistent with clinical results in breast cancer, disease still progressed while animals were on treatment (Fig. 1C). Moreover, we evaluated the efficacies of two covalent FGFR inhibitors, FIIN4 and futibatinib, in the highly metastatic, FGFR dependent 4T1 model of MBC (Fig. S1). Covalent inhibition of FGFR reduced 4T1 tumor growth, but complete tumor regression could not be achieved before reaching dose-limiting toxicity (Fig. S1). In addition to these in vivo approaches, we also compared the efficacies of FGFR kinase inhibitors in the 4T07 cell model growing in a 3D spheroid assay. This 3D culture approach combines tumor spheroid formation in a non-adherent round bottom dish followed by placement of the spheroid onto a bed of matrix[31]. Our results demonstrate that 100 nM of these compounds significantly decreased the growth of 4T07 3D spheroids irrespective of exogenous FGF2 (Fig. 1D). We also utilized the 3D spheroid approach to evaluate these compounds against the D2.A1 cells, a murine model of *FGFR1*-amplified MBC[32]. Unlike the 4T1 and 4T07 cells, addition of exogenous FGF2 is required to induce signaling downstream of FGFR and this event can be effectively blocked by pretreatment with FGFR kinase inhibitors (Fig. S2)[8]. The addition of exogenous FGF2 significantly stimulates growth of D2.A1 spheroids, and this was prevented by all FGFR kinase inhibitors tested (Fig. 1E). These data suggest complete and on-target inhibition of ligand-induced cell growth at these concentrations. To further investigate the efficacy of FGFR kinase inhibitors, we tested them using the D2.OR cell model of systemic dormancy. Similar to their D2.A1 counterparts, the D2.OR cells express high levels of FGFR1, but these cells stop growing when they are removed from traditional two-dimensional culture and are placed in compliant 3D matrixes[33]. We have recently demonstrated the 3D growth of the D2.OR cells can be rescued by exogenous addition of FGF2[32]. Here, the addition of FGF2 similarly induced the outgrowth of D2.OR spheroids in a compliant matrix (Fig. 1F). Addition of FGFR kinase inhibitors again prevented this ligand-induced spheroid growth, but trypsinization of these spheroids and return to 2D culture resulted in colony formation by residual viable cells (Fig. 1G). Cellular recovery from the spheroid assay was variable, preventing quantification, but viable cells were always recovered from the spheroid assay, irrespective of indicated treatment conditions. Taken together, these data indicate that targeted inhibition of FGFR kinase activity effectively blocks ligand-induced cell growth but fails to eliminate residual cells.

Formation of G-quadruplex in the FGFR1 proximal promoter

Given the limitations of only inhibiting the enzymatic activity of FGFR and the established kinase-independent functions of FGFR, we sought to evaluate alternate means of targeting this important oncogenic system. Examination of the *FGFR1* proximal promoter identified three potential G-quadruplex-forming sequences S1-S3 (Fig. 2A). To analyze the folding topology and thermal stabilities of these putative G-quadruplex forming sequences, we used circular dichroism (CD) spectroscopy (Fig. 2B). A positive peak at 264 nm and a negative peak at 245 nm in the CD spectra of S1 and S3 sequences indicate the formation of parallel G-quadruplex structures, whereas the two positive peaks at 265 nm and 295 nm suggest a hybrid conformation for S2 (Fig. 2C)[34]. CD-melting experiments showed that both S1 and S3 G-quadruplex structures are stable far above physiological temperatures with a melting temperature notably higher than S2 (Fig. 2D). Based on these results, we conclude that the S1 and S3 elements in the *FGFR1* proximal promoter region are the predominant locations for G-quadruplex formation and these structures can be stabilized by CX-5461 (Fig. 2E).

G-quadruplex stabilization inhibits FGFR1 expression

Given that the *FGFR1* proximal promoter contains G-quadruplex forming elements, we next investigated if small molecule ligands designed to bind to and stabilize G-quadruplex could impede FGFR1 expression. To this end, we tested the effect of the G-quadruplex binder, CX-5461, on the thermal stability of *FGFR* promoter G-quadruplex. Using CD melting experiments, we showed that CX-5461 stabilized the major *FGFR1* G-quadruplex formed in the S1 and S3 elements by 16 °C and 23 °C, respectively (Fig. 2D). We next evaluated the impact of CX-5461 on FGFR1 expression in the BT549 model of *FGFR1* amplified triple-negative breast cancer. CX-5461 and a structurally similar compound, quarfloxin, both downregulated FGFR1 expression at the mRNA and protein levels as much as or more as compared to inhibition of c-Myc expression, a known target of G-quadruplex regulation (Fig. 3A–D)[35]. Further confirming G-quadruplex-mediated regulation of FGFR1, we observed that FGFR1 expression is also inhibited by the G-quadruplex-binding molecule TMPyP4 but not by its position-isomer TMPyP2, which does not bind G-quadruplex (Fig. 3E). In addition to blocking constitutive expression of *FGFR1*, we also found that G-quadruplex stabilization was able to inhibit EMT-induced expression of *FGFR1* driven by ectopic expression of the master EMT transcription factor Twist (Fig. S3).

To more directly examine the regulatory functions of G-quadruplex in the *FGFR1* proximal promoter, we constructed luciferase reporters driven by truncated *FGFR1* promoter sequences containing the major G-quadruplex forming elements, S1 and S3 (Fig. 4A). The absolute transcriptional activity of both constructs was similar and highly active as compared to a 'promoterless' control (Fig. 4B). Consistent with our observed inhibition of endogenous *FGFR1* expression, the transcriptional activity of both reporter constructs was significantly inhibited upon CX-5461 treatment (Fig. 4C). Given that similar transcriptional activity and CX-5461 inhibition was observed with the S3 sequence alone, we sought to disrupt G-quadruplex formation in this construct. Importantly, mutation of the S3 sequence to prevent G-quadruplex-forming capability abolished the ability of CX-5461 to inhibit luciferase reporter activity (Figs. S4 and 4D). Taken together, these findings suggest that the *FGFR1* proximal promoter forms G-quadruplex that can be stabilized by CX-5461, limiting transcription.

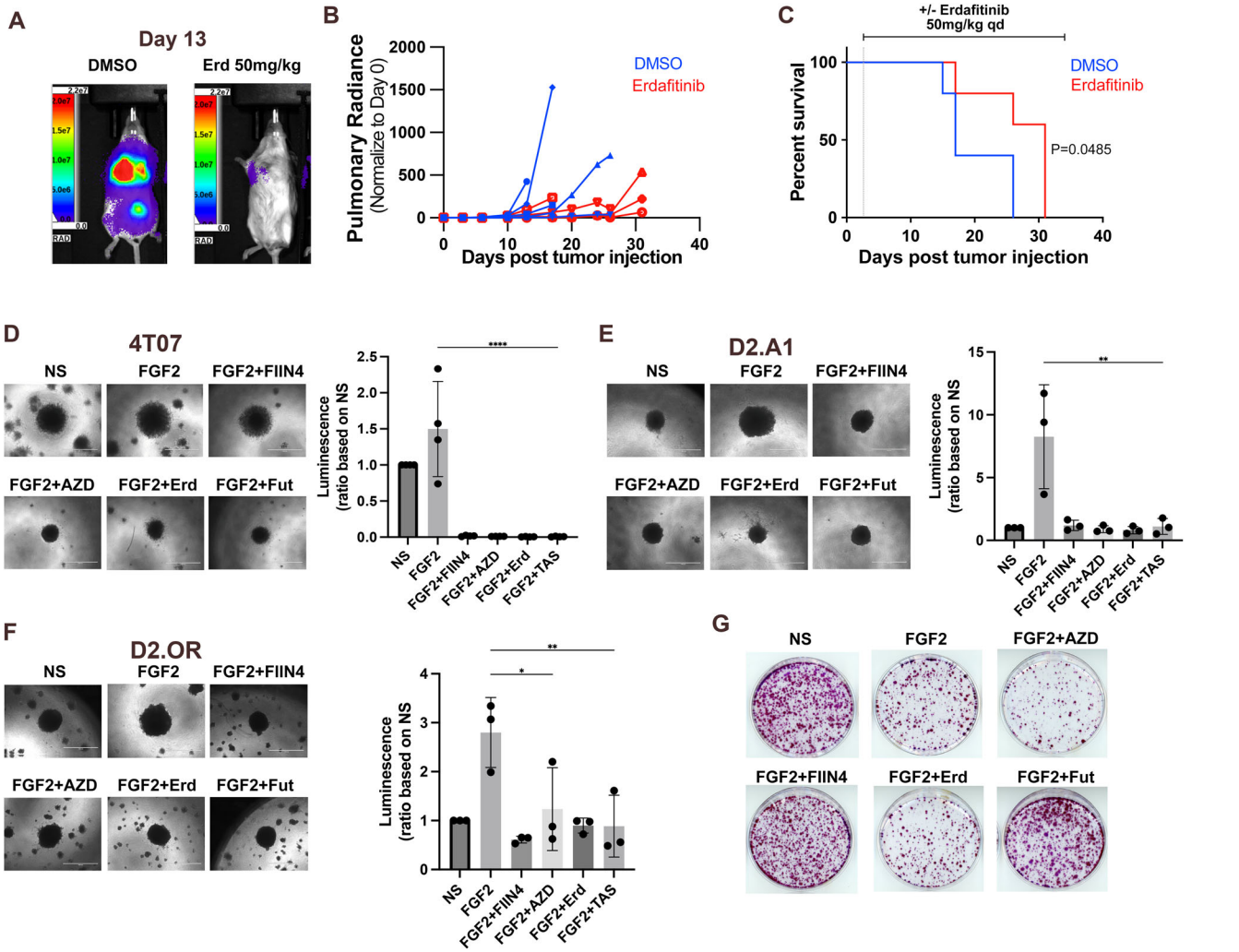

Fig. 1 | Inhibition of FGFR kinase activity suppresses tumor growth but fails to eliminate dormant breast cancer cells. A Representative bioluminescence imaging (BLI) images of control and erdafitinib (Erd) treated (50 mg/kg/po/qd) mice bearing 4T07 pulmonary tumors monitored by bioluminescence 13 days following tail vein inoculation. **B** Bioluminescent values from pulmonary regions of interest (ROI) were normalized to the values at the initial day of injection. Data are the individual values for each mouse ($n = 5$) per treatment group. **C** Kaplan-Meier analyses of control and erdafitinib treated mice, bearing 4T07 pulmonary tumors, resulting in the indicated p-value. **D** 4T07 spheroids expressing luciferase were formed in non-adherent round bottom plates and then plated onto a bed of matrix in the presence or absence of FGF2 (20 ng/ml) or the indicated FGFR inhibitors (100 nM). **E** D2.A1 cells expressing luciferase were similarly used in spheroid culture, treated, and analyzed as in panel **D**. **F** D2.OR cells expressing luciferase were similarly used in spheroid culture, treated, and analyzed as in panels **D** and **E**. Luminescence values at day 6 were normalized to the non-stimulated (NS) conditions. Scale bars in panels **D**–F are 1000 µm. Data are the mean ± s.e.m. ($n \geq 3$) where $^*p < 0.05$. **G** Following 3D culture, D2.OR spheroids were trypsinized and single cells were plated on tissue culture plastic. Colony formation in 10 cm^2 tissue culture dishes was visualized by crystal violet staining 14 days later as a measure of dormant cell survival.

G-quadruplex stabilization can block FGF-induced growth and eliminate dormant cells

In addition to human TNBC cells, we also evaluated the impact of CX-5461 on *FGFR1* expression in the D2.A1 murine model of *FGFR1*-amplified metastatic breast cancer. While the S1 sequence is not conserved between human and mouse, the S3 G-quadruplex sequence is identical between human and mouse. We utilized our fibronectin (FN)-coated tissue culture scaffolds to obtain protein samples from CX-5461 treated cells as this allowed for up to 4 days of treatment without significantly affecting cell viability of the D2.A1 cells (Fig. 5A, B)[6]. This approach clearly demonstrated that *FGFR1* expression is reduced by CX-5461 treatment in this physiologic growth environment (Fig. 5C). To quantitatively interrogate the functional importance of reducing *FGFR1* expression levels, we again utilized our 3D spheroid assay where growth of D2.A1 3D spheroids can be significantly enhanced through addition of exogenous FGF2 (Fig, 5D). Concomitant treatment with either the FGFR kinase inhibitor erdafitinib or CX-5461 completely blocked FGF2-induced spheroid growth (Fig. 5D). Consistent with our results in Fig. 1, use of the D2.OR dormancy model demonstrated the ability of erdafitinib to block FGF2-induced spheroid growth, a result that could also be obtained using CX-5461 (Fig. 5E). However, unlike erdafitinib, CX-5461 also eliminated residual cell survival as determined by colony formation after the spheroids were plated back to 2D Cell culture (Fig. 5F). These results demonstrate that unlike enzymatic inhibitors of FGFR kinase activity, CX-5461 effectively prevents FGF2-induced cell growth and reduces the survival of residual BC cells.

In vivo application of CX-5461 reduces FGFR1 expression and blocks pulmonary tumor formation

We next sought to determine if the in vivo application of CX-5461 could reduce *FGFR1* expression and block tumor growth in a metastatic site. We have previously demonstrated that genetic depletion of *FGFR1* inhibits pulmonary tumor formation by the D2.A1 cells[6]. Therefore, mice were inoculated with D2.A1 cells via the lateral tail vein to allow for pulmonary seeding (Fig. 6A). Three days after the cells were injected, mice were treated

A

```
3900 CCCGGCCAAC TCTTTTCTTA AATTAGCCAG GGAGGCGTGG GTGGGTTGGG TGAGGAGTTG GGTGGGGGGA TCTCATTCAG TATTCAAACT TCTACAAGTT
4000 TCGGGGTTGA GGTGGGTGAT GGTAAGGGAA CAGGCCCTGC CACTACCTTT CATAGTGACT TCCATTTGTG TAATATTTTT GGTCCACTGA GAGCTATTAT
4100 TTTATTTGAT TCTTATGACC ATCTTGTGAA GGAGTATCAA CAGATACCCC GTTTTGATTT TATCAGATGC ATGATTTGTC CTACATCAAA CTTCATAAAT
4200 GATGGACAGA ATGGAGGAAT CCTTCAGACC AAGTGCTGCC TACTTCCCAC CCCAATGGTG GCCTCAGCCT GGGCTCACAT CACACGCCCC AAGGAGCCTT
4300 GGAAAAAATA AAGGCTCTTG GCTCCTTCCT GGGACAGCGT GATTCCTCAT GTCTGAGCAG GCCCATGAAC TTGTATTTTT CAGACGTTCC CTAGGACCCG
4400 TGTCCATCTG GATTAGGGAA CCACTACATT ATACCACTTC GCGGGAAGAC TCAGGGGGAA GCATTTTAGC CACTTTCCTG TGTTCCACAG TACTGGAGGG
4500 TGTTCTGAGT GGGCTGTGAT TAATTTCCAA ACCAACCACA CGTCTCCCCT CAACTCCCAC TGCTTACTCT TTGCTTCCTA GACATTCACT GCAGGCTGGA
4600 GACTTCTGGA AGCCAACAGC ATCGCTGTAG AATTTACAGG GTCCAGTTCC CGGTGGACCA CAAAACCTAA ATTATGTGGC TGGGGAAAGC TGAAATCCAA
4700 GGGAAGGGTT TGAGGAGGGG CTGACCTTAT AATAAAACCG GCTTGTATTT ACTAAGTGTT AACTATGCGC TAGGCCCTCG TTGACGCCTC AACTCTATGT
4800 GAAAAGCACT ATTATCCCCC ATTTACAGAT GGGAAAACAG AGATTTAGAG CGCGAAAATC ATTTCCCCAA GGCGCACAGA CTCCAAAGCC CACGCTACCA
4900 GGTACAACCT CAAGGCTGCG GCGTCTCTTC ACCTGCCCCC TAGCCCCCAA ACCGCTGCTA TGTCTAGGGC CTGACATTCC GGCGCCCTCT GGGACGTGCT
5000 CAGATGCAGG GGCGCAAACG CCAAAGGAGA GGAAGAGAAG GGCAGAGCGC CGGACAGCTC GGCCCGCTCC CCGTCCTTTG GGGCCGCGGC CCAGGCTGTA
5100 TGGGGAACTA CAAGGCCCAG CAGGCAGCTG CAGGGGGCGG AGGCGGAGGA GGGACCAGCG CGGGTGGGAG TGAGAGAGCG AGCCCTCGCG CCCCGCCGGC
5200 GCATAGCGCT CGGAGCGCTC TTGCGGCCAC AGGCGCGGCG TCCTCGGCGG CGGGCGGCAG CTAGCGGGAG CCGGGACGCC GGTGCAGCCG CAGCGCGCGG
```

TSS

B

	Sequences	[K⁺] (mM)	Melting Temperature (°C)
S1	5'-CA **GGG** A **GG** CGT **GGG** T **GGG** TT **GGG** TGA **GG** AGTT **GGG** T **GGGGGG** AT-3'	100	65.0
S1a	5'-CA **GGG** A **GG** CGT **GGG** T **GGG** TT **GGG** TGA **GG** AGTT-3'	100	64.5
S2	5'-AA **GGG** AA **GGG** TTTGA **GG** A **GGGG** CT-3'	100	47.5
S3	5'-CA **GGGGG** C **GG** A **GG** C **GG** A **GG** A **GGG** ACCAGCGC **GGG** T **GGG** AGT-3'	100	60.3
S3a	5'-CA **GGGGG** C **GG** A **GG** C **GG** A **GG** A **GGG** ACCA-3'	100	43.9

C

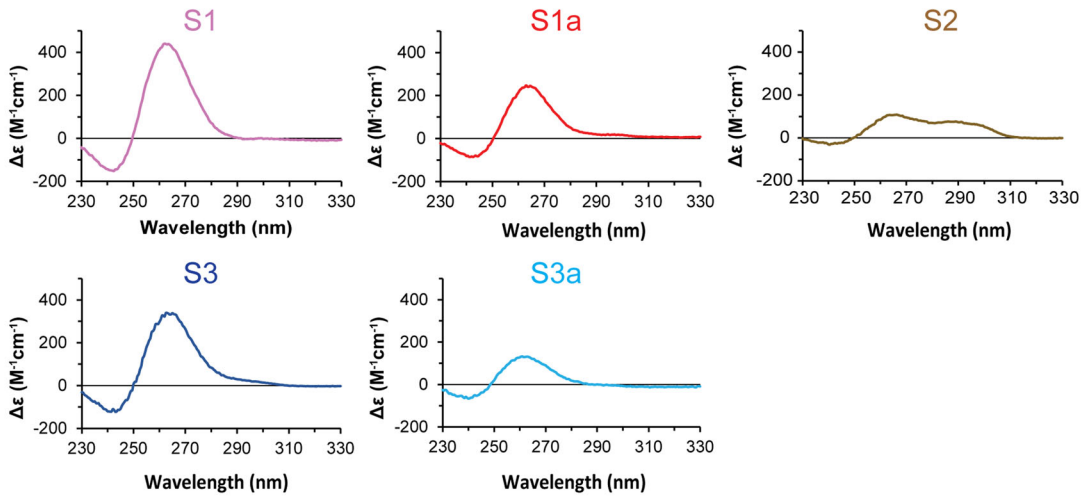

D

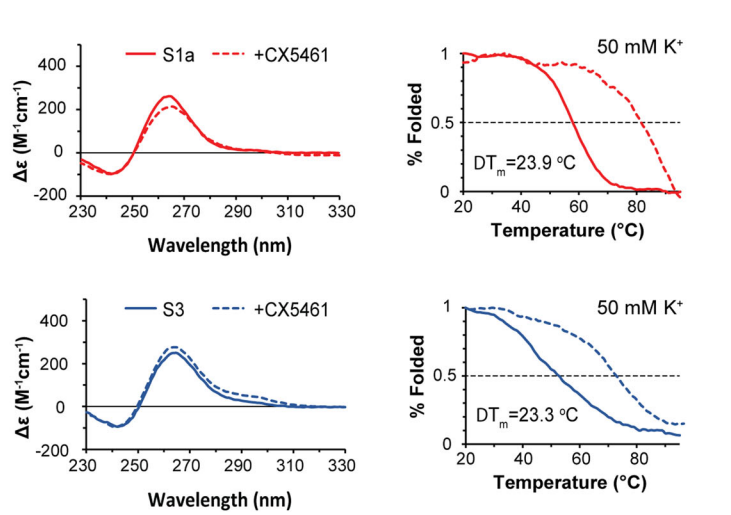

E

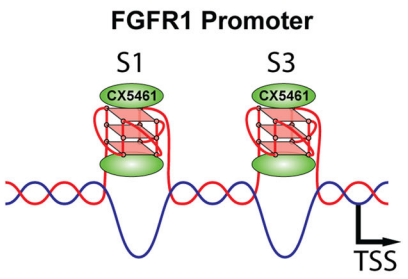

Fig. 2 | Formation of G-quadruplex in the *FGFR1* proximal promoter. A The *FGFR1* (−1300/+100) proximal promoter with potential G-quadruplex forming sequences indicated in colored text. The transcriptional start site (TSS) is indicated by the red arrow. **B** Sequences of putative G-quadruplex forming sequences and their melting temperatures. **C** Circular dichroism (CD) spectra of the G-quadruplex forming sequences noted in panel B in the presence of 100 mM K^+. **D** CD spectra and melting curves of S1 and S3 G-quadruplex forming sequences in the presence and absence of the G-quadruplex stabilizing compound, CX-5461, in the presence of 50 mM K^+. **E** Schematic representation of the G-quadruplex formation in the *FGFR1* promoter and stabilization by CX-5461 impedes transcription.

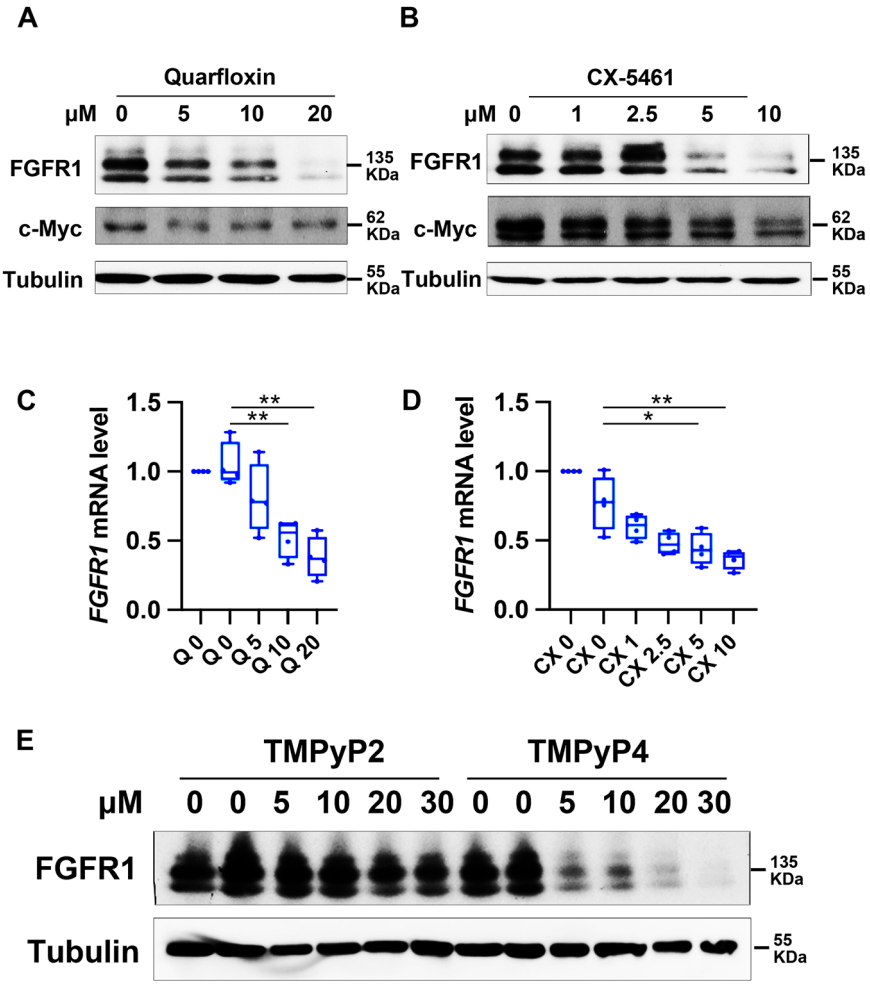

Fig. 3 | G-quadruplex stabilization inhibits FGFR1 expression. A, **B** Immunoblot analyses for *FGFR1* and *c-Myc* expression in the BT549 cells upon treatment with the G-quadruplex stabilizers, quarfloxin (A) or CX-5461 (B), for 24 h. **C**, **D** RT-PCR for *FGFR1* transcript levels in BT549 cells after treatment with the indicated G-quadruplex stabilizers, quarfloxin (**C**) and CX-5461 (**D**), for 24 h. Data are normalized to FGFR1 levels in the untreated control cells and are the mean ±s.e.m. of four independent experiments ($n = 4$) resulting in the indicated p-values where $^{*}p > 0.05$ and $^{**}p > 0.01$. **E** Immunoblot analyses for *FGFR1* expression in the BT549 cells upon treatment with the G-quadruplex stabilizer, TMPyP4, for 24 h. Similar treatment with the structural analog TMPyP2 that does not bind G-quadruplex was used as a control.

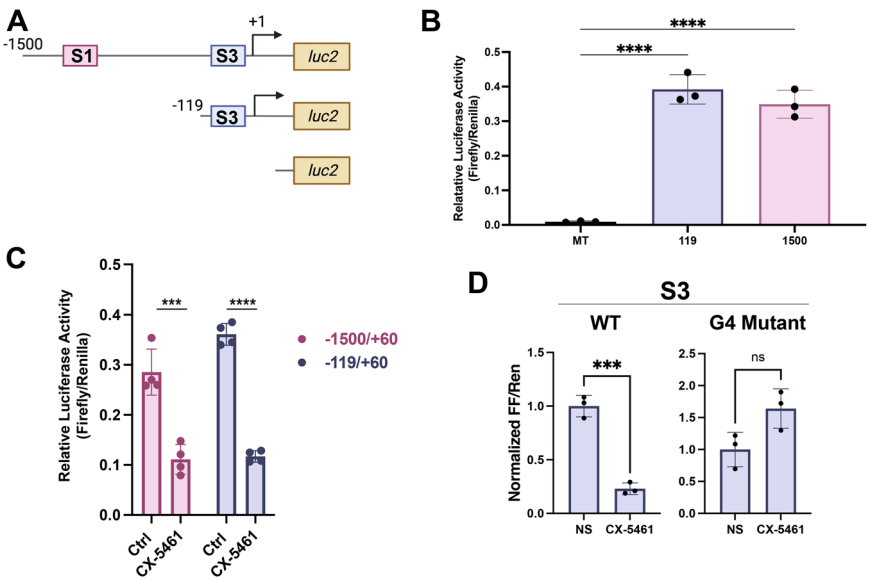

Fig. 4 | CX-5461 suppresses *FGFR1* proximal promoter activity. A Truncated *FGFR1* proximal promoter regions were cloned into the pGL4.2 luciferase reporter vector. The G-quadruplex forming sequences from Fig. 2 are noted as S1 and S3. **B** Dual-Glo luciferase assay showing different lengths of *FGFR1* proximal promoter activity in HEK293T cells. Data are normalized to the ratio of firefly luciferase to renilla from pGL4.2 empty vector and are the mean ±s.e.m. ($n = 3$). **C** Dual-Glo luciferase assay showing *FGFR1* proximal promoter activity in HEK293T cells in the presence or absence of 1 μM CX-5461 for 72 hours ($n = 4$). **D** The sequential G sequences in S3 of the −119/+60 luciferase construct were replaced with thymidine and adenine (G4 mutant) to prevent G-quadruplex formation. Reporter activity in response to CX-5461 treatment was assessed as above ($n = 3$ biologically independent experiments, with each dot representative of the average of 4 technical repeats). In panels B-D, $^{**}p < 0.05$, $^{***}p < 0.01$, $^{****}p < 0.001$.

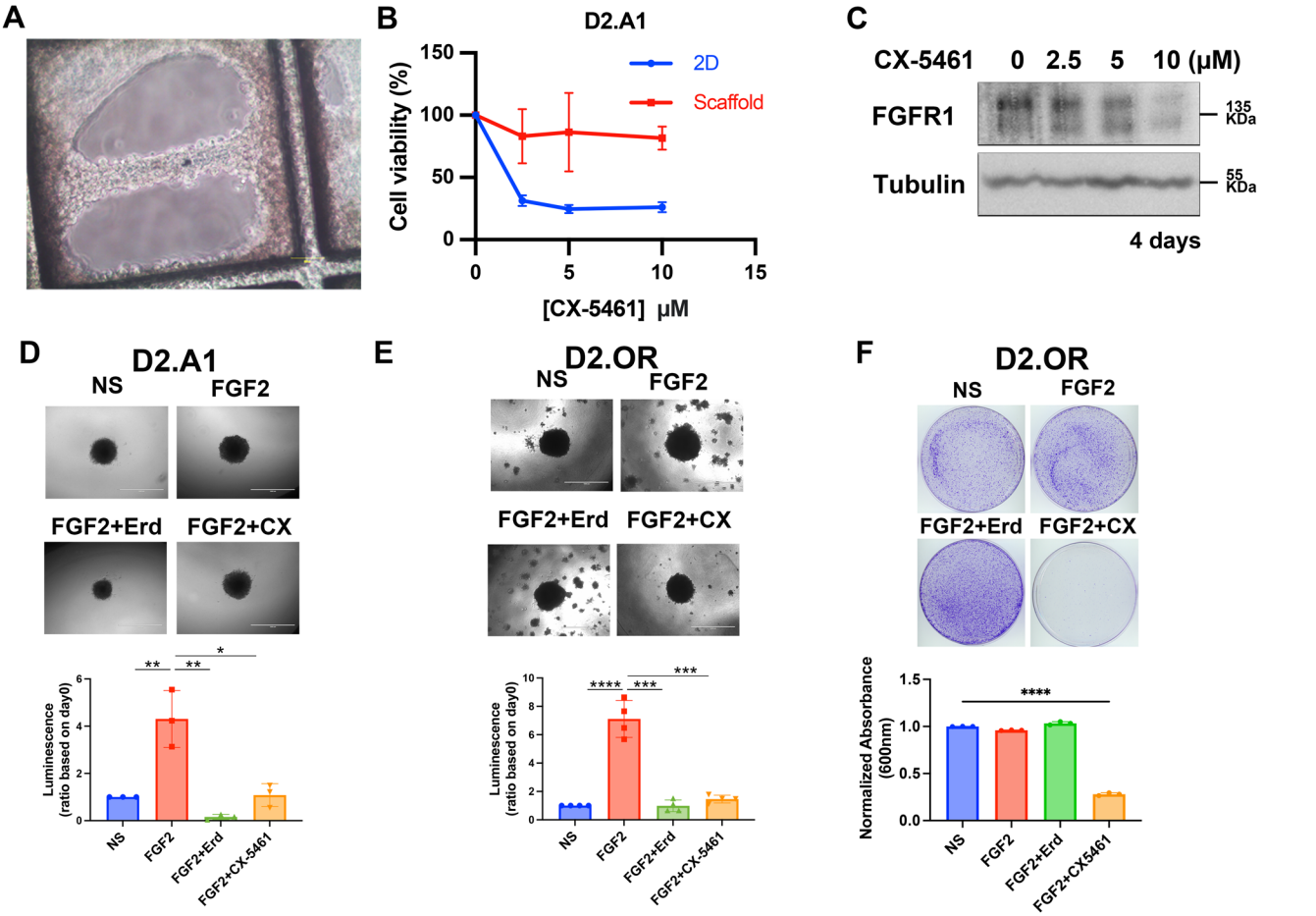

Fig. 5 | CX-5461 targets *FGFR1* expression and eliminates residual breast cancer cells. A Image of D2.A1 cells cultured on fibronectin fibrils that span unsupported space between the culture scaffold grids is taken 4 days after plating cells. Scale bar is 50 μm. **B** D2.A1 cells were cultured on FN-coated scaffolds or standard tissue culture plastic (2D) for 6 days in the presence of the indicated concentrations of CX-5461 and cell viability was measured ($n = 3$). **C** Immunoblot analyses for *FGFR1* following 4 days treatment with the indicated concentrations of CX-5461. **D** D2.A1 spheroids expressing firefly luciferase were formed in a round bottom plate and then transferred to a bed of matrix in the presence or absence of 20 ng/ml FGF2, 100 nM Erdafitinib (Erd), or 100 nM CX-5461 (CX). Scale bars are 1000 μm. Following 6 days of culture bioluminescence was measured and treated values were normalized to non-stimulated (NS) spheriods. Data are the mean ±s.e.m. ($n = 3$). **E** As in panel D, firefly luciferase expressing D2.OR cells were used in a spheroid growth assay. Scale bars are 1000 μm. **F** Following 3D culture, D2.OR spheroids were disassociated and single cells were plated on tissue culture plastic. Colony formation in 10cm^2 tissue culture dishes was visualized by crystal violet staining after 14 days and cells were solubilized and read at an absorbance 600 nm. For all panels $^*p < 0.05$, $^{**}p < 0.01$, $^{***}p < 0.001$, and $^{****}p < 0.0001$.

with CX-561 for 21 days (Fig. 6A). Treatment with CX-5461 resulted in a significant reduction in pulmonary tumor formation as determined by bioluminescent imaging and enumeration of pulmonary tumor nodules upon necropsy (Fig. 6B–F). This antitumor-affect was achieved without causing overt toxicity as animal weights remained similar in both the treated and untreated groups (Fig. 6D). Consistent with our in vitro data, both immunohistochemistry (IHC) and immunoblot analyses of dissected pulmonary nodules demonstrated a marked reduction in *FGFR1* protein levels in tumors derived from CX-5461 treated mice (Fig. 6G–I). In addition to these pharmacodynamic endpoints, we also conducted a survival analysis. Here, mice were again inoculated with D2.A1 cells via the lateral tail vein and allowed to seed for 3 days. These tumor bearing animals were treated either with the FGFR kinase inhibitor, erdafitinib, CX-5461, or both compounds for a period of 10 days and subsequently monitored for survival (Fig. 7A). This transient treatment with CX-5461 effectively delayed pulmonary growth as compared to the control and erdafitinib treated groups, as determined by bioluminescent imaging (Fig. 7B). No additional benefit in terms of tumor burden or survival was gained by combining erdafitinib with CX-5461, but the combination did cause animal weight loss suggestive of increased toxicity (Fig. 7B–D). Taken together, these findings clearly demonstrate that CX-5461 effectively blocked the growth of an *FGFR1*-driven model of breast cancer while growing within the pulmonary microenvironment.

Discussion

FGFR1 drives breast cancer disease progression by supporting cell survival, angiogenesis, migration, and invasion[36]. Amplification of the *FGFR1* gene locus correlates with decreased breast cancer patient survival[37,38]. Hence, FDA-approved FGFR-targeted kinase inhibitors have been evaluated in MBC[10]. However, unlike cancers driven by activating mutations in FGFRs, *FGFR1*-amplified MBC patient response to enzymatic inhibitors is limited. Consistent with these clinical data, our evaluation of different FGFR kinase inhibitors in mouse models of MBC indicates that pulmonary tumors can quickly overcome FGFR kinase inhibition leading to disease progression[30].

More broadly, intrinsic and acquired resistance to kinase inhibitors is a major clinical challenge in cancer[3]. FGFR seems to be no exception as mutation of the active site and other epigenetic mechanisms are at play in driving intrinsic and acquired resistance to FGFR kinase inhibitors[39,40]. Herein, we utilized an immune-competent model of *FGFR1*-amplified MBC to demonstrate that a prolonged benefit from an FDA-approved FGFR kinase inhibitor is not achievable and limited by treatment-induced toxicity. We have previously demonstrated that the FGFR kinase inhibitors

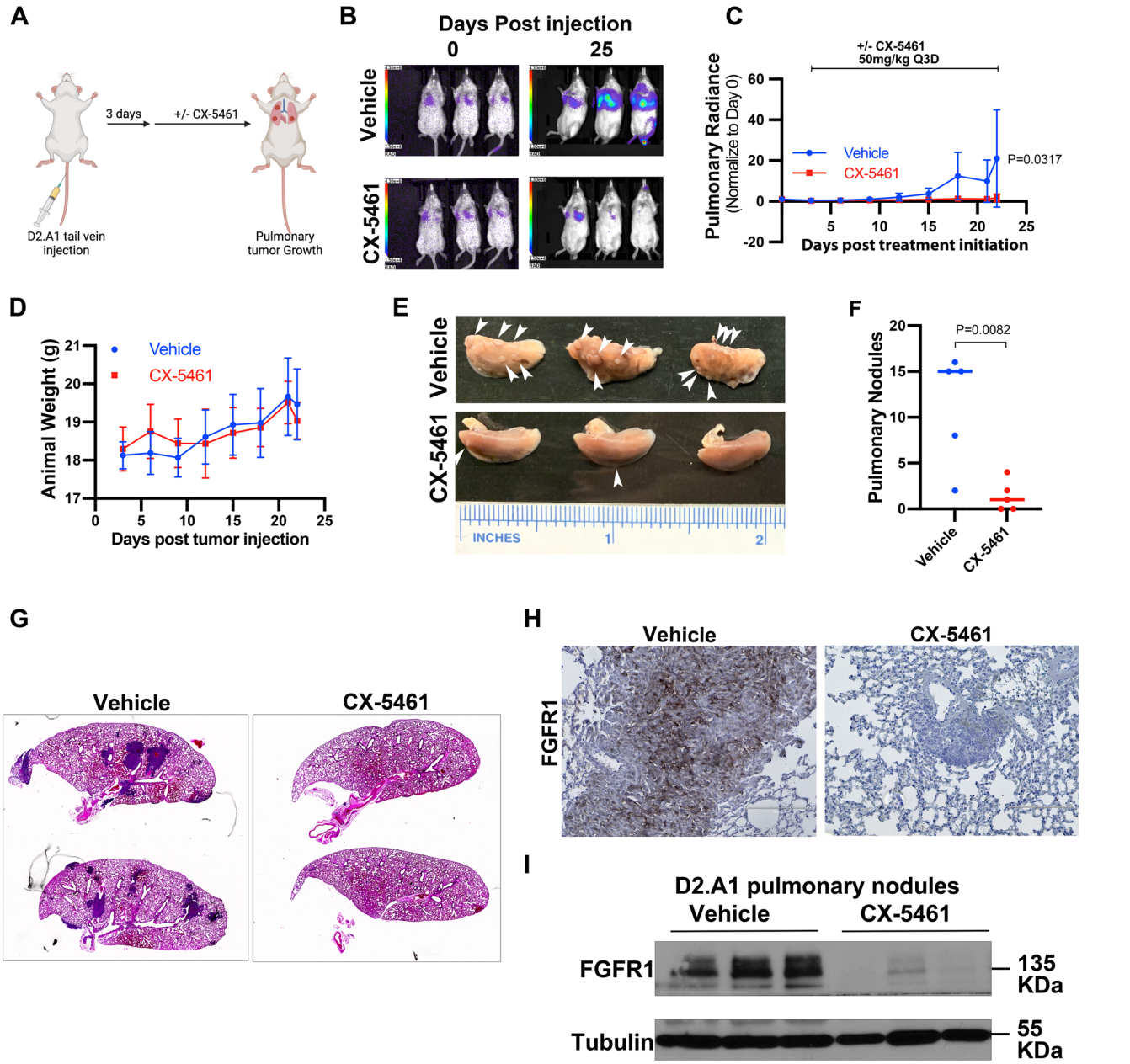

Fig. 6 | CX-5461 therapy reduces *FGFR1* expression and inhibits pulmonary tumor formation. A Schematic representation of pulmonary delivery of D2.A1 cells followed by treatment with CX-5461 (Created with BioRender.com). **B** Representative BLI images immediately after delivery of D2.A1 cells (day 0) and 25 days post tumor inoculation for control animals (vehicle) and those that received CX-5461. **C** Bioluminescent values from pulmonary ROI were normalized to the values at the initial day of injection. Data are the mean ± s.e.m. of 5 mice per treatment group resulting in the indicated *p*-value ($n = 5$). **D** Body weights of mice from vehicle and CX-5461 treated groups ($n = 5$). **E** Photos of fixed lungs harvested from control (vehicle) and CX-5461 treated animals. Macroscopic pulmonary tumor nodules are indicated by arrow heads. **F** Quantification of pulmonary tumor nodules identified in vehicle and CX-5461 groups. $n = 5$ mice per group resulting in the indicated *p*-value. **G** Representative pulmonary H&E staining of one lobe, from 2 mice in the control (vehicle) and CX-5461 treated groups. **H** IHC staining for FGFR1 in pulmonary histological sections from vehicle and CX-5461 treated mice. Scale bar are 150 µm. **I** Immunoblot analyses of *FGFR1* protein levels in isolated lung nodules from vehicle and CX-5461 treated mice ($n = 3$).

cause weight reduction of mice, data that are consistent with the numerous toxicities that have been reported in human patients[41]. Many of the established toxicities associated with FGFR kinase inhibitors are linked to on-target inhibition of FGFRs 1–4[41].

We also demonstrate that FGFR kinase inhibitors fail to target residual tumor leaving a population of cells capable of reestablishing disease upon cessation of treatment. While the mechanistic explanations for the shortcomings of FGFR kinase targeting are not definitively defined, FGFR1 nuclear translocation and upregulation of other growth factor receptors can contribute to resistance[15,42]. Hence, an epigenetic therapy that can subvert these mechanisms of kinase inhibitor resistance would benefit *FGFR1*-amplified MBC patients.

Through analysis of the *FGFR1* proximal promoter, we discovered G-quadruplex forming elements that could be stabilized by the G-quadruplex binding small molecule, CX-5461[27]. Although not detectable in our systems, previous studies have also identified G-quadruplex formation in the FGFR2 promoter[43]. Indeed, application of CX-5461 both in vitro and in vivo clearly inhibits *FGFR1* promoter activity and effectively

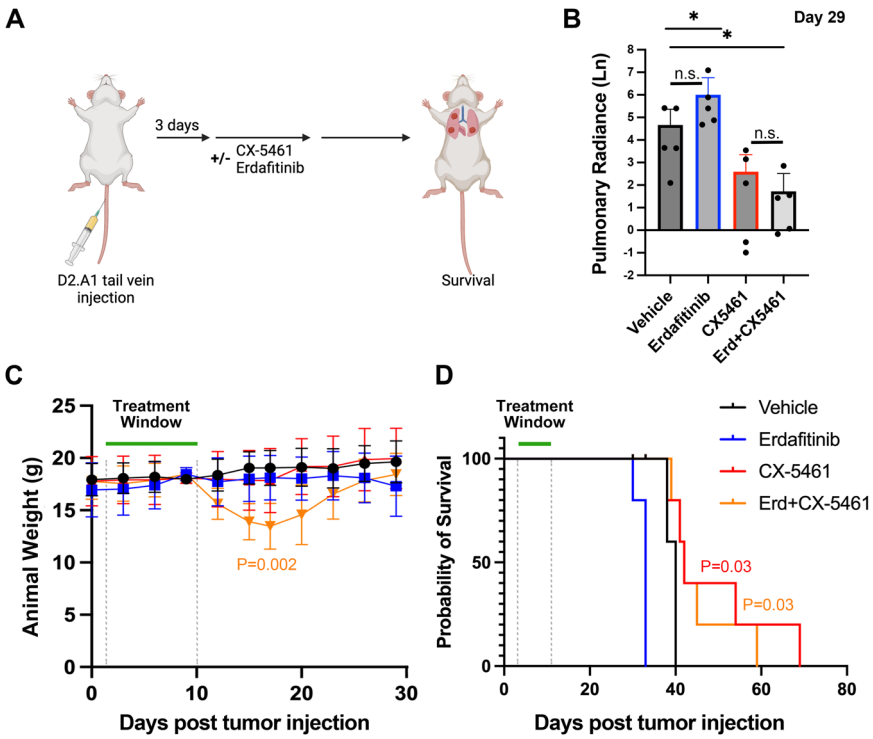

Fig. 7 | CX-5461 therapy prolongs survival of pulmonary tumor bearing animals. A Schematic representation of pulmonary delivery of D2.A1 cells followed by treatment with CX-5461 and/or erdafitinib (Created with BioRender.com). **B** Bioluminescent values from pulmonary ROI were normalized to the values at the initial day of injection. Data are the mean ±s.e.m. of 5 mice per treatment group where $^*p < 0.05$ ($n = 5$). **C** Body weights of mice from vehicle, erdafitinib and CX-5461 treated groups ($n = 5$). **D** Survival analyses of mice bearing D2.A1 pulmonary tumors. As above, mice received the vehicle as a control or were treated with erdafitinib and/or CX-5461 for the indicated amount of time. Kaplan-Meier plot comparing survival of the vehicle and CX-5461 treatment groups ($n = 5$ mice per group). Data were analyzed using a log-rank test, resulting in the indicated *p*-values.

normalizes FGFR1 expression levels. Therefore, we conclude that G-quadruplex is forming in the *FGFR1* proximal promoter and stabilization of these three-dimensional structures limits transcription. Our findings demonstrate that CX-5461 stabilizes at least two G-quadruplex forming elements within 1500 base pairs of *FGFR1* TSS. We termed these elements: S1 and S3. The S1 sequence is specific to the human *FGFR1* promoter region, but S3 is conserved in both human and mouse. Hence, G-quadruplex-regulated expression of this critical growth factor receptor appears to be conserved across species.

Similar to targeted inhibition of kinase activity, reduction of *FGFR1* expression by G-quadruplex stabilization suppressed FGF ligand-induced spheroid growth, but also reduced dormant cell viability. The complete mechanism of how CX-5461 eliminates dormant cells remains to be established. However, previous studies suggest synergy in targeting c-MYC and PDGFR in combination with FGFR, all factors that are connected to G-quadruplex and simultaneously repressed upon treatment with CX-5461[18,41,42,44,45]. While our data does not indicate a benefit of combining CX-5461 with erdafitinib, this combination may still be a valid approach, particularly in the *MYC*-amplified tumors. Finally, CX-5461 also has inhibitory activity against topoisomerase II and has been linked to the inhibition of DNA repair[28,46,47]. The pleotropic ability of CX-5461 to normalize oncogene expression along with its additional pharmacology likely contributes to its ability to act as a potent anti-cancer agent. Importantly, our data, in conjunction with clinical data, demonstrate that the anti-cancer activity of CX-5461 is accomplished with acceptable systemic toxicity, comparatively less than what was observed upon pan-inhibition of FGFR kinase activity.

Overall, our studies are consistent with clinical observations demonstrating intrinsic resistance of MBC to FGFR tyrosine kinase inhibitors. We identify G-quadruplex forming sequences in the *FGFR1* promoter region which can be stabilized via the G-quadruplex ligand, CX-5461, normalizing FGFR1 expression. The use of biochemical and functional assays indicates that CX-5461 limits FGFR1 signaling and abrogates dormant cell survival. Our study strongly supports evaluation of CX-5461 or similar G-quadruplex-targeting agents as therapeutics for MBC patients, particularly those harboring *FGFR1* amplification.

Methods

Cell lines and reagents

D2-HAN (D2.A1 and D2.OR), 4T1 derivatives (4T1 and 4T07) were obtained from Fred Miller (Wayne State University, Detroit, MI) and cultured in DMEM containing 10% fetal bovine serum (FBS) and 1% Pen/Strep. Normal murine mammary gland (NMuMG) cells and their derivatives were cultured in DMEM supplemented with 10% FBS, 1% Pen/Strep, and 10 μg/ml of insulin. BT549 cells were cultured in RPMI-1460 supplemented with 10% FBS, 1% Pen/Strep, and 10 μg/ml of insulin. MCF10A cells were cultured in 1:1 DMEM (Corning Mediatech, Inc.) and F12 (Corning Mediatech, Inc.) supplemented with 29 mM HEPES (Amresco, LLC), 10 mM sodium bicarbonate (Macron), 5% horse serum (Sigma), 10 μM/mL insulin, 10 ng/mL epidermal growth factor (EGF) (Gold Biotechnology), 0.5 μg/mL hydrocortisone (Sigma), 100 ng/mL cholera toxin (Sigma), and 1% antibiotics (100 units/ml penicillin and 100 g/ml streptomycin; Corning Mediatech) at 37 °C in a humidified atmosphere in a 5% CO_2 incubator.

NMuMG and MCF10A cells expressing YFP and Twist were constructed through stable transduction using pBabe and pMSCV viral particles as previously described[7,48]. Bioluminescent D2-HAN derivates, 4T1 derivatives were engineered to stably express luciferase by transfection with pNifty-CMV-luciferase. All cell lines are regularly tested for mycoplasma contamination through PCR.

In vivo therapeutic assays

D2.A1 (1×10^6) and 4T07 (5×10^5) were delivered into the lateral tail vein of 4 to 6-week-old BALB/c female mice purchased from Jackson Laboratories. FGFR kinase inhibitors were administered through oral gavage with the indicated concentrations once per day. CX-5461 was administered in 50 mM NaH_2PO_4 at 50 mg/kg orally every 3 days. FGFR inhibitors and G-quadruplex ligand manufacturers and gavage formulations are listed as supplementary Table 1. Pulmonary tumor formation was monitored via bioluminescent imaging after intraperitoneal injection of luciferin through AMI HT (Spectral Instruments). The lungs were fixed overnight by 10% formaldehyde (Fisher) after sacrificing the mice and then stored in 80% ethanol. Paraffin sectioning at 5μm thickness and H&E staining were

conducted by AML laboratories, Inc. (Jacksonville, FL). The images of lung sections were obtained by Cytation 5 cell imaging multi-mode reader with Gen5 software (BioTek Instruments, Inc.). All in vivo assays have complied with all relevant ethical regulations for animal use were conducted under IACUC approval from Purdue University. No randomization or blinding was done.

3D spheroid assay

Breast cancer cells (4×10^3) were plated in 96-well, ultra-low attachment and round bottom plates (Corning) in full growth media and cultured for a week. Afterward, the spheroids were transferred with 50 µL residual media to 96-well flat clear bottom white wall plates with a bed of 50 µL growth factor reduced basement membrane hydrogel and 150 µL fresh media containing 5% basement membrane hydrogel with FGF2 and/or FGFR inhibitors. Luminescence of spheroids was detected, and media was replenished every three days. For analyses of residual cell survival, the D2.OR spheroids were trypsinized, transferred to 100 mm 2D culture dishes, and colonies were stained with crystal violet culture after 14 days.

Circular dichroism spectroscopy

CD experiments were run on a Jasco J-1100 spectropolarimeter (JASCO Inc.) equipped with a temperature-controlled cell holder and stirrer. DNA (Sigma-Aldrich) was dissolved in 10 mM K^+ buffer (2.5 mM potassium phosphate, 7.5 mM KCl, pH 7) to obtain 3–5 µM samples and annealed by heating to 95 °C for 5 minutes, followed by overnight cooling at room temperature. CD spectra were measured at 25 °C over a spectral range of 230–330 nm with a 10-mm quartz cuvette. The spectral parameters were: a scanning rate of 50 nm/min, 1.0 nm data pitch, 1.0 nm bandwidth, a response time of 1 s, and 5 accumulations. The spectra were blank corrected by subtracting a spectrum of the buffer. CD melting experiments were performed by monitoring the ellipticity at 264 nm over a temperature range of 20–95 °C. The heating rate was 1 °C/min and data points were recorded every 0.5 °C, while the samples were continuously stirred at 200 rpm. Melting temperatures, T_m, were determined by locating the intersection of the median line between the upper and lower baseline and the melting curve. CD melting experiments were run in duplicate. Spectra and melting curves were also obtained in the presence of CX-5461 (AdooQ BioScience) with a 5:1 ligand:DNA ratio.

Immunoblotting

The procedure of immunoblotting was conducted as previously described[48]. G-quadruplex stabilizers were used at the indicated concentrations and times in MBC cell lines. The antibodies used were described in supplementary table 2. Immunoblot results were obtained via chemiluminescence or fluorescent secondaries and detected with either X-ray film or via the LI-COR odyssey system.

mRNA transcript analyses

For real-time PCR analysis, metastatic breast cancer cells were treated with G-quadruplex stabilizers at indicated different time points. Afterward, total RNA was isolated using the E.Z.N.A HP total RNA kit (Omega). Total RNA was subsequently transcribed using the Verso cDNA synthesis kit (Thermo Scientific), and semiquantitative real-time PCR was performed via Maxima SYBR Green (Thermo Scientific) as described previously. The primers used in this study were listed in supplementary table 3.

Luciferase reporter assay

The proximal promoter regions of the human *FGFR1* gene relative to the transcriptional initiation site were cloned from BT549 genomic DNA by PCR and inserted into pGL4.2 vector (Promega, Madison, MA). The primers used for cloning were listed in supplementary table 3. The predicted G-quadruplex formation sequences were analyzed via web-based server QGRS Mapper. The vector containing the mutated S3 G4 sequence detailed in supplementary fig. 4 was constructed by VectorBuilder. The vector ID VB221205-1315fht can be used to retrieve detailed information about the vector on vectorbuilder.com. For all reporter assays, HEK293T cells were transiently transfected overnight with LT1 liposomes (Mirus, Madison, WT), which contained 2.3 µg/well of firefly luciferase vectors and 0.2 µg/well of pcDNA3.1 encoding renilla luciferase under the control of the CMV promoter. Afterward, the cells were treated with CX-5461 for 72 h and subsequently harvested and assayed for firefly and renilla luciferase using the Dual-glo Assay System (Promega).

Immunohistochemistry

Formalin-fixed and paraffin-embedded tissue sections were deparaffinized with xylene and rehydrated with decreasing concentration of ethanol. Antigen retrieval was achieved by boiling in 10 mmol/L sodium citrate buffer (pH 6.0). These processed sections were incubated with antibodies specific for FGFR1 overnight at 4 °C. Staining was detected using the anti-rabbit biotinylated secondary antibodies in combination with ABC (Vector) and DAB reagents (Vector). The manufacturers of the antibodies were listed in supplementary table 2. These sections were then counterstained with hematoxylin (Fisher), dehydrated through ethanol and xylene, and cover-slipped via a xylene-base mounting medium.

Statistics and reproducibility

A two-tail Student's *t* test was used for comparing the difference between two groups of data in the in vitro assays. Error bars identify the standard error of the mean. For in vivo experiments, the measurements were compared with a Mann–Whitney non-parametric test. Survival analysis was performed via GraphPad Prism 9 software, and the distributions of survival were compared by a log-rank test.

Reporting summary

Further information on research design is available in the Nature Portfolio Reporting Summary linked to this article.

Data availability

All data generated or analyzed during this study are included in this published article (and its supplementary data 1 file).

Received: 11 September 2023; Accepted: 18 July 2024;
Published online: 09 August 2024

References

1. Dillekås, H., Rogers, M. S. & Straume, O. Are 90% of deaths from cancer caused by metastases? *Cancer Med* **8**, 5574–5576 (2019).
2. Attwood, M. M., Fabbro, D., Sokolov, A. V., Knapp, S. & Schiöth, H. B. Trends in kinase drug discovery: targets, indications and inhibitor design. *Nat. Rev. Drug Discov.* **20**, 839–861 (2021).
3. Pottier, C. et al. Tyrosine Kinase Inhibitors in Cancer: Breakthrough and Challenges of Targeted Therapy. *Cancers (Basel)* **12**, 731 (2020).
4. Razavi, P. et al. The Genomic Landscape of Endocrine-Resistant Advanced Breast Cancers. *Cancer Cell* **34**, 427–438.e6 (2018).
5. Yates, L. R. et al. Genomic Evolution of Breast Cancer Metastasis and Relapse. *Cancer Cell* **32**, 169–184.e7 (2017).
6. Wendt, M. K., Taylor, M. A., Schiemann, B. J., Sossey-Alaoui, K. & Schiemann, W. P. Fibroblast growth factor receptor splice variants are stable markers of oncogenic transforming growth factor β1 signaling in metastatic breast cancers. *Breast Cancer Res* **16**, R24 (2014).
7. Brown, W. S. et al. FGFR signaling maintains a drug persistent cell population following epithelial-mesenchymal transition. *Oncotarget* **7**, 83424–83436 (2016).
8. Brown, W. S., Tan, L., Smith, A., Gray, N. S. & Wendt, M. K. Covalent Targeting of Fibroblast Growth Factor Receptor Inhibits Metastatic Breast Cancer. *Mol. Cancer Ther.* **15**, 2096–2106 (2016).
9. Liu, L. et al. Reductions in Myeloid-Derived Suppressor Cells and Lung Metastases using AZD4547 Treatment of a Metastatic Murine Breast Tumor Model. *Cell. Physiol. Biochem.* **33**, 633–645 (2014).

10. Nogova, L. et al. Evaluation of BGJ398, a Fibroblast Growth Factor Receptor 1-3 Kinase Inhibitor, in Patients With Advanced Solid Tumors Harboring Genetic Alterations in Fibroblast Growth Factor Receptors: Results of a Global Phase I, Dose-Escalation and Dose-Expansion Study. *J. Clin. Oncol.* **35**, 157–165 (2017).
11. Sobhani, N. et al. Current Status of Fibroblast Growth Factor Receptor-Targeted Therapies in Breast Cancer. *Cells* **7**, 76 (2018).
12. Servetto, A., Formisano, L. & Arteaga, C. L. FGFR signaling and endocrine resistance in breast cancer: Challenges for the clinical development of FGFR inhibitors. *Biochim Biophys. Acta Rev. Cancer* **1876**, 188595 (2021).
13. Santolla, M. F. & Maggiolini, M. The FGF/FGFR System in Breast Cancer: Oncogenic Features and Therapeutic Perspectives. *Cancers (Basel)* **12**, 3029 (2020).
14. Coleman, S. J. et al. Nuclear translocation of FGFR1 and FGF2 in pancreatic stellate cells facilitates pancreatic cancer cell invasion. *EMBO Mol. Med* **6**, 467–481 (2014).
15. Dunham-Ems, S. M. et al. Fibroblast Growth Factor Receptor-1 (FGFR1) Nuclear Dynamics Reveal a Novel Mechanism in Transcription Control. *Mol. Biol. Cell* **20**, 2401–2412 (2009).
16. Chioni, A.-M. & Grose, R. FGFR1 cleavage and nuclear translocation regulates breast cancer cell behavior. *J. Cell Biol.* **197**, 801–817 (2012).
17. Du, G. et al. Discovery of a Potent Degrader for Fibroblast Growth Factor Receptor 1/2. *Angew. Chem. Int. Ed.* **60**, 15905–15911 (2021).
18. Chen, L., Dickerhoff, J., Sakai, S. & Yang, D. DNA G-Quadruplex in Human Telomeres and Oncogene Promoters: Structures, Functions, and Small Molecule Targeting. *Acc. Chem. Res.* **55**, 2628–2646 (2022).
19. Brown, R. V. et al. The Consequences of Overlapping G-Quadruplexes and i-Motifs in the Platelet-Derived Growth Factor Receptor β Core Promoter Nuclease Hypersensitive Element Can Explain the Unexpected Effects of Mutations and Provide Opportunities for Selective Targeting of Both Structures by Small Molecules To Downregulate Gene Expression. *J. Am. Chem. Soc.* **139**, 7456–7475 (2017).
20. Wu, G., Xing, Z., Tran, E. J. & Yang, D. DDX5 helicase resolves G-quadruplex and is involved in MYC gene transcriptional activation. *Proc. Natl Acad. Sci.* **116**, 20453–20461 (2019).
21. Wang, K.-B. et al. Indenoisoquinoline Topoisomerase Inhibitors Strongly Bind and Stabilize the MYC Promoter G-Quadruplex and Downregulate MYC. *J. Am. Chem. Soc.* **141**, 11059–11070 (2019).
22. Brooks, T. A. & Hurley, L. H. The role of supercoiling in transcriptional control of MYC and its importance in molecular therapeutics. *Nat. Rev. Cancer* **9**, 849–861 (2009).
23. Carvalho, J., Mergny, J.-L., Salgado, G. F., Queiroz, J. A. & Cruz, C. G-quadruplex, Friend or Foe: The Role of the G-quartet in Anticancer Strategies. *Trends Mol. Med.* **26**, 848–861 (2020).
24. Balasubramanian, S., Hurley, L. H. & Neidle, S. Targeting G-quadruplexes in gene promoters: a novel anticancer strategy? *Nat. Rev. Drug Discov.* **10**, 261–275 (2011).
25. Yang, D. & Okamoto, K. Structural insights into G-quadruplexes: towards new anticancer drugs. *Future Med Chem.* **2**, 619–646 (2010).
26. Alessandrini, I., Recagni, M., Zaffaroni, N. & Folini, M. On the Road to Fight Cancer: The Potential of G-Quadruplex Ligands as Novel Therapeutic Agents. *Int. J. Mol. Sci.* **22**, 5947 (2021).
27. Xu, H. et al. CX-5461 is a DNA G-quadruplex stabilizer with selective lethality in BRCA1/2 deficient tumours. *Nat. Commun.* **8**, 14432 (2017).
28. Xu, H. & Hurley, L. H. A first-in-class clinical G-quadruplex-targeting drug. The bench-to-bedside translation of the fluoroquinolone QQ58 to CX-5461 (Pidnarulex). *Bioorg. Med Chem. Lett.* **77**, 129016 (2022).
29. Wendt, M. K. et al. TGF-β stimulates Pyk2 expression as part of an epithelial-mesenchymal transition program required for metastatic outgrowth of breast cancer. *Oncogene* **32**, 2005–2015 (2013).
30. Akhand, S. S. et al. Pharmacological inhibition of FGFR modulates the metastatic immune microenvironment and promotes response to immune checkpoint blockade. *Cancer Immunol. Res* **8**, 1542–1553 (2020).
31. Ali, R., Brown, W., Purdy, S. C., Davisson, V. J. & Wendt, M. Biased signaling downstream of epidermal growth factor receptor regulates proliferative versus apoptotic response to ligand. *bioRxiv 352526* https://doi.org/10.1101/352526 (2018).
32. Kulkoyluoglu Cotul, E. et al. FGFR1 Signaling Facilitates Obesity-Driven Pulmonary Outgrowth in Metastatic Breast Cancer. *Mol. Cancer Res* **22**, 254–267 (2024).
33. Wendt, M. K., Taylor, M. A., Schiemann, B. J. & Schiemann, W. P. Down-regulation of epithelial cadherin is required to initiate metastatic outgrowth of breast cancer. *Mol. Biol. Cell* **22**, 2423–2435 (2011).
34. Del Villar-Guerra, R., Trent, J. O. & Chaires, J. B. G-Quadruplex Secondary Structure Obtained from Circular Dichroism Spectroscopy. *Angew. Chem. Int Ed. Engl.* **57**, 7171–7175 (2018).
35. Siddiqui-Jain, A., Grand, C. L., Bearss, D. J. & Hurley, L. H. Direct evidence for a G-quadruplex in a promoter region and its targeting with a small molecule to repress c-MYC transcription. *PNAS* **99**, 11593–11598 (2002).
36. Ali, R., Akhand, S. S. & Wendt, M. K. Targeting FGFR for the Treatment of Breast Cancer. In *Resistance to Targeted Therapies in* Breast *Cancer* (ed. Prosperi, J. R.) vol. 16 117–137 (Springer International Publishing, Cham, 2017).
37. Turner, N. et al. FGFR1 Amplification Drives Endocrine Therapy Resistance and Is a Therapeutic Target in Breast Cancer. *Cancer Res.* **70**, 2085–2094 (2010).
38. Elbauomy Elsheikh, S. et al. FGFR1 amplification in breast carcinomas: a chromogenic in situ hybridisation analysis. *Breast Cancer Res* **9**, R23 (2007).
39. Krook, M. A. et al. Efficacy of FGFR Inhibitors and Combination Therapies for Acquired Resistance in FGFR2-Fusion Cholangiocarcinoma. *Mol. Cancer Therapeutics* **19**, 847–857 (2020).
40. Englinger, B. et al. Lipid droplet-mediated scavenging as novel intrinsic and adaptive resistance factor against the multikinase inhibitor ponatinib. *Int J. Cancer* **147**, 1680–1693 (2020).
41. Kommalapati, A., Tella, S. H., Borad, M., Javle, M. & Mahipal, A. FGFR Inhibitors in Oncology: Insight on the Management of Toxicities in Clinical Practice. *Cancers (Basel)* **13**, 2968 (2021).
42. Servetto, A. et al. Nuclear FGFR1 regulates gene transcription and promotes antiestrogen resistance in ER+ breast cancer. *Clin. Cancer Res* https://doi.org/10.1158/1078-0432.CCR-20-3905 (2021).
43. Zhang, L., Tan, W., Zhou, J., Xu, M. & Yuan, G. Investigation of G-quadruplex formation in the FGFR2 promoter region and its transcriptional regulation by liensinine. *Biochimica et. Biophysica Acta (BBA) - Gen. Subj.* **1861**, 884–891 (2017).
44. Kaiser, C. E., Gokhale, V., Yang, D. & Hurley, L. H. G-Quadruplex-Mediated Transcriptional Regulation of PDGFR-β. *Top. Curr. Chem.* **330**, 1–21 (2013).
45. Chen, Y. et al. The Major G-Quadruplex Formed in the Human Platelet-Derived Growth Factor Receptor β (PDGFR-β) Promoter Adopts a Novel Broken-Strand Structure in K+ Solution. *J. Am. Chem. Soc.* **134**, 13220–13223 (2012).
46. Pan, M. et al. The chemotherapeutic CX-5461 primarily targets TOP2B and exhibits selective activity in high-risk neuroblastoma. *Nat. Commun.* **12**, 6468 (2021).
47. Hilton, J. et al. Results of the phase I CCTG IND.231 trial of CX-5461 in patients with advanced solid tumors enriched for DNA-repair deficiencies. *Nat. Commun.* **13**, 3607 (2022).

48. Abdullah, A. et al. Epigenetic targeting of neuropilin-1 prevents bypass signaling in drug-resistant breast cancer. *Oncogene* **40**, 322–333 (2021).

Acknowledgements
This work was supported by the National Cancer Institute (R01CA271597, R01CA232589, R01CA177585, and U01CA240346). We also acknowledge the support of the Purdue Institute for Cancer Research via its NIH NCI grant (P30CA023168). We also acknowledge personnel and the use of the facilities within the Bindley Bioscience Center, a core facility of the NIH-funded Indiana Clinical and Translational Sciences Institute.

Author contributions
H.L. and M.H.S. contributed to the writing and preparation of the manuscript, conceptualized, and conducted experiments. S.W., S.S.A., J.D., M.M., and M.A. conducted experiments. L.S. conceptualized experiments and contributed key reagents. D.Y. and M.K.W. conceptualized experiments and contributed to the writing and preparation of the manuscript.

Competing interests
The authors declare no competing interests.

Additional information
Supplementary information The online version contains supplementary material available at https://doi.org/10.1038/s42003-024-06602-x.

Correspondence and requests for materials should be addressed to Danzhou Yang or Michael K. Wendt.

Peer review information *Communications Biology* thanks Alberto Servetto and the other, anonymous, reviewer(s) for their contribution to the peer review of this work. Primary Handling Editors: Myron Evans II and Dario Ummarino.